Aerodynamic Simulation and Optimization of Micro Aerial Vehicle Rotor Airfoil at Low Reynolds Number

Sushil Nepal[1], Zhao Qijun[2], Wang Bo[3], Md. Kamruzzaman[4] and Suraj Adhikari[5]

[1,2,3&4]College of Aerospace Engineering, Nanjing University of Aeronautics and Astronautics, Nanjing, China
[5]School of Mechanical Engineering, Nanjing University of Science and Technology, Nanjing, China
E-mail: nepalsushil@outlook.com, zhaoqijun@nuaa.edu.cn, wangbo@nuaa.edu.cn,
kamruzzamanshafi@outlook.com, sura_adhikari1991@outlook.com

Abstract - This paper describes the aerodynamic simulation and optimization of NACA 0012 airfoil at a low Reynolds number using unsteady Reynolds-averaged Navier-Stokes (URANS) and Spalart–Allmaras turbulence model in Ansys Fluent. The purpose of this paper is to simulate and optimize the airfoil to get better aerodynamic performances at low Reynolds numbers. The Parsec method was selected for the optimization of the NACA 0012 airfoil. Both of these airfoils are simulated using CFD Fluent between 0 to 13-degree angle of attack at a low Reynolds number of 200000. To simulate the airfoil, mesh generation is crucial so an O-grid structured mesh is created. After the simulation, several aerodynamic performances are compared between the airfoils, such as lift coefficient, drag coefficient, pressure coefficient, and lift-to-drag ratio. And the calculated results from Xfoil are taken as references. Between NACA 0012 and optimized NACA 0012, the optimized airfoil showed better aerodynamic performances than the normal one, which was the goal of this paper. Later on, the different flow field variables, such as density, temperature, pressure, and vorticity magnitude were analyzed and compared. Both the airfoils at a different angle of attack were analyzed for these functions, like 7°, 11°, and 20° AOA. During the analytical process, Q-criterion appears to be a very important method of vortex identification in the flow field. With this analysis, we came to know, that as the angle of attack increases the adverse pressure gradient also increases, which creates a big reverse flow.

Keywords: Simulation, Optimization, URANS, Spalart-Allmaras, CFD, Aerodynamic Performances

Nomenclature

MAV   Micro Aerial Vehicle
UAV   Unmanned Aerial Vehicle
CFD   Computational Fluid Dynamics
AOA   Angle of Attack

I. INTRODUCTION

A smaller-scale air vehicle (MAV), or miniaturized scale flying vehicle, is a class of little UAVs that has a size limitation and might be self-ruling. MAVs have been working for interest purposes, for example, aeronautical, mechanical technology challenges, and elevated photography. Because of the advancement of the technologies, people are not only interested in electric motors but it has also enabled the broad adoption of small-scale aircraft for different terrestrial applications. Numerous Micro Aerial Vehicles (MAVs) and small Unmanned Aerial Vehicles (UAVs), both civil and military, are in use today. Operation at their design flight condition often requires rotors, propellers, or wings to perform at Reynolds numbers significantly below 500,000. The chord-based Reynolds number for these small-scale rotors usually requires knowledge of airfoil performance at even lower Reynolds numbers [1].

The MAV wings are derived from airfoils, and the aerodynamic forces are defined by the airfoil's lifting and drag coefficients. Due to relative fluid motion, accurate and efficient determination of the aerodynamic forces on wings is vital for the design and production of MAVs. Since the flow separation property at a high Reynolds number is either delayed or none, it is more reliable and convenient to analyze and forecast the characteristics of the flows than at a lower Reynolds number. Moreover, at lower Reynold numbers there isn't strong force or energy for the flow to tackle the adverse pressure gradient, the fluid particles might have the possibility of separation, which is not a case in higher Reynold numbers. This leads to the transition from a laminar to a turbulent regime. Thus, the particle gains energy and reattaches to the surface, forming a bubble, which is called the separation bubble. At higher angles of attack, these effects become more predominant where the conventional model fails to predict the physics of the flow. Since the ultra-low Reynolds number has many practical applications and it is an exciting field of study, scientists are doing more research on it [2].

The history of an unmanned aerial vehicle with a span of about 15cm and weight not more than 150g is not so long ago. In the 1990s, these types of UAVs were born, and nowadays, they are also known as Micro Aerial Vehicles or MAVs. There has been a huge improvement in technology these days, which is also having a positive impact on the field of aerodynamics, as we can see different aircraft and drones are being built for difficult purposes. The smaller sizes and dimensions of MAVs need a better understanding of the physics involved in them, compared to traditional aircraft, which is a continuing research subject. This work has caught the interest of many people as well as the aviation industries,

which is to examine this low number of flight Reynolds and the problems it presents. The researchers are inspired by these technologies to have different experiments and trials for better comprehension of different kinds of MAVs at lower Reynolds numbers [3]. This paper aims to simulate an airfoil at a low Reynolds number. Different aerodynamic characteristics of an aforementioned airfoil will be compared with reference values. At last, the optimization of the airfoil will take place to get better aerodynamic performance, and these airfoils can be used to design the MAV wings.

Fig. 1 MAVs

II. LITERATURE REVIEW

With increasing uses of MAVs in different aspects, researchers are working diligently to develop MAVs with improved characteristics that will suit the present-day environment and requirements. Researchers are also trying to make positive changes in the Low Reynolds number field with different airfoils that can be used in MAVs to make things easier and faster. There are still many unanswered questions regarding the low Reynolds number MAV. Still, the previous studies on it have inspired many people to work in this field and make MAVs valuable in Urban settings, tunnels, and caves. Some research has already been completed in this area, which is enough to do more advanced investigations.

Low Reynold numbers MAVs need to have better aerodynamic performance; to understand their characteristics, a test has been completed at a range of different Reynolds numbers. As an initial study of the architecture of MAV, two-dimensional numerical simulations were carried out at three separate Reynolds numbers for 70,000, 100,000 & 120,000. The MAVs whose linear dimension is not more than 150mm would operate at a lower altitude, and this is the suitable range of the Reynolds number where we can conduct the experiments for surveillance or other purposes. Eppler with reflex camber is used to design this special type of airfoil, which is supposed to provide a lower pitching moment value. The results of the current study are that the aerodynamic efficiency at a low Reynolds number is not so good as the drag increases and lift decreases. But the reflex camber profile used here makes this airfoil demonstrate a stable longitudinal pitching moment. For the MAV, these kinds of behaviors are pretty much desirable. The result of this work was as expected. As anticipated, pitching moment coefficient variation with increasing angle of attack indicates longitudinal stability till about 12 degrees. After which there is instability indicating stall condition. Such behavior is especially desirable for the operation of a MAV configuration, which facilitates a more straightforward design in terms of pitching control devices [4].

A different work has been carried out on low Reynolds numbers for analyzing the effect of leading and trailing edge flaps on the flat plate airfoils. Reynolds numbers 40000, 60000, and 80000 were chosen to conduct the test. By visualizing the on and off-the-surface flow, numeric data were complemented. The results showed that the leading and trailing edge flaps deployment could enhance the airfoil performance significantly, not just compared with a flat plate but also with a 5% camber circular arc profile. The optimal leading and trailing edge flap angle was taken as 15 degrees. In this test increasing the Reynolds number showed significant improvement in the performance of the conventional airfoils [5].

The research on the design of Low Reynolds Number Airfoil for Micro Aerial Vehicle was also done, and the result was quite impressive. Using XFLR5 software and the adopted Foil Direct Design process, the new airfoil is created by modifying the airfoil parameters, that is, maximum thickness, max camber, thickness position, and camber, based on the maximum lift coefficient. The new airfoil's aerodynamic characteristics are tested and checked against the reference airfoil, such as FX63137sm, S1223, and e423. The number of Reynolds ranges between 342000 and 1028000. It is evident from this work that a low Reynolds number airfoil can be designed to achieve a much higher maximum lift coefficient than the reference airfoil. Software, like XFLR5, uses the direct design process, which is always beneficial to obtain the high lift performance of the airfoil. The practical design of an airfoil has demonstrated applications of this

philosophy with a low Reynolds number, which achieved a maximum lift coefficient Clmax = 2.53 at the mentioned Reynolds number [6].

III. AERODYNAMIC ANALYSIS METHOD FOR AIRFOIL

CFD or Computational Fluid Dynamics is a widely used method to predict and analyze the fluids flow. And the same method is used here to analyze the aerodynamic performance of the aorfoils. It uses different techniques to solve these problems, such as physics, computer science, mathematics, and many more. There are different kinds of predictions, such as quantitative and qualitative predictions; the CFD method tends to solve problems with the help of these predictions [7]. Before solving any kind of problem, CFD needs to plan, understand, and construct before predicting any result, and it does so by using different mathematical models, numerical computation, and software, which will effectively solve the problems. In any kind of scenario, from weather forecasting to designing an airplane or its wing, the calculation of the motion of gases or liquids is a vital job, and CFD helps to solve all these difficulties. Another essential part of using CFD is, that you always have to keep in mind the accuracy of the results. Sometimes for a sophisticated design where it can take hours of calculation, if you want to get an accurate result and reduce the computational time, using parallel processing would be a good option. If you want to run thousands of iterations for a complex design on a normal desktop, parallel processing will help solve the problems accurately and in significantly less amount of time. CFDs are utilized as an option in contrast to real experimentation since it gives a reasonable method for perception and experimentation. Utilizing reproductions, CFDs permit researchers, designers, and experts to watch numerous situations dependent on wanted estimations, and have the option to arrive at increasingly precise resolutions. The purpose of this is CFDs empower the reproductions of examinations, which in actuality would be excessively costly, hard to lead, or unthinkable given the conditions.
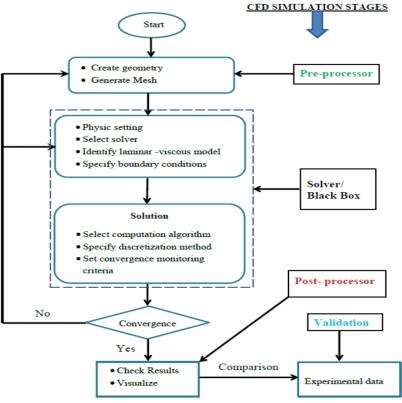

Fig. 2 CFD Simulation Stages

There are several advantages of CFD, which attracted people to use this cost-effective method. CFD offers quick results for complex modeling geometry and allows the study of tough structures in a more visualized way. For a better, sophisticated, and manageable study of fluid flow, CFD provides a reasonable option fruitfully as it converts actual fluids into digital imagery. Not only that, but it also provides ways to solve problems that are challenging for the experiment. Having such decent advantages, there are some drawbacks that CFD has, such as the outcome of the different physical models could be fluctuated. Sometimes it takes you to such a situation where there is a dead end, and it is tough to find a way out of it, which leads an inaccurate and unacceptable results [8]. Several equations control the CFD simulation. They are known as governing equations. The continuity equation, momentum equation, and energy equation form overall governing equations, which are given by equations (1), (2), and (3). Equation (2) only represents the x-component of the momentum equation. Similarly, the y-component and z-component can be established [9].

$$\frac{\partial \rho}{\partial t} + \nabla \cdot (\rho \vec{V}) = 0$$

(1)

$$\frac{\partial(\rho u)}{\partial t} + \nabla \cdot (\rho u \vec{V}) = -\frac{\partial p}{\partial x} + \frac{\partial \tau_{xx}}{\partial x} + \frac{\partial \tau_{yx}}{\partial y} + \frac{\partial \tau_{zx}}{\partial z} + \rho f_x$$

(2)

$$\frac{\partial}{\partial t}\left[\rho\left(e + \frac{V^2}{2}\right)\right] + \nabla \cdot \left[\rho\left(e + \frac{V^2}{2}\vec{V}\right)\right]$$
$$= \rho\dot{q} + \frac{\partial}{\partial x}\left(k\frac{\partial T}{\partial x}\right) + \frac{\partial}{\partial y}\left(k\frac{\partial T}{\partial y}\right)$$
$$+ \frac{\partial}{\partial z}\left(k\frac{\partial T}{\partial z}\right) - \frac{\partial(up)}{\partial x} - \frac{\partial(vp)}{\partial y} - \frac{\partial(wp)}{\partial z} + \frac{\partial(u\tau_{xx})}{\partial x}$$
$$+ \frac{\partial(u\tau_{yx})}{\partial y} + \frac{\partial(u\tau_{zx})}{\partial z} + \frac{\partial(v\tau_{xy})}{\partial x} + \frac{\partial(v\tau_{yy})}{\partial y} + \frac{\partial(v\tau_{zy})}{\partial z}$$
$$+ \frac{\partial(w\tau_{xz})}{\partial x} + \frac{\partial(w\tau_{yz})}{\partial y} + \frac{\partial(w\tau_{zz})}{\partial z} + \rho\vec{f}\cdot\vec{V}$$

(3)

IV. MESH GENERATION

While performing the CFD simulation, many things play key roles, and generating quality mesh is one of them. It is a very crucial part of the CFD simulation of any design, either 2D or 3D. In the CFD simulation, the accuracy of the results depends upon the mesh quality. Orthogonality, skewness, and smoothness are the parameters that help to provide quality mesh [10]. For this paper, a structural O-grid mesh is generated. A structural mesh is characterized by regular connectivity, which can be represented as an array of two or three dimensions. This limits the option of elements to 2D quadrilaterals or 3D hexahedra. For CFD analysis, the ultimate goal is to create a high-quality mesh, which gives superior results too. The grid density for the mesh is 300*150. 150 points each are used in the top and bottom wall of the airfoil, along with 10 points on the trailing edge. The original NACA 0012 airfoil of chord length 1m with a blunt trailing edge was used for 2D simulation. The NACA 0012 profile is one of the oldest and certainly the most tested of all airfoils; it has been simulated in dozens of separate wind tunnels over more than 50 years. The diversity and availability of experimental results for this symmetric, 12%-thick airfoil make it a good choice to be used as a validation benchmark for numerical simulations [11].
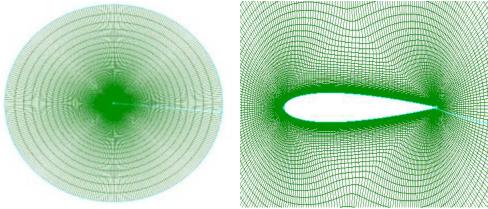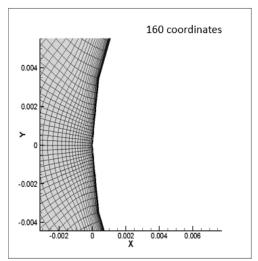

Fig. 3 O-grid Structured mesh

First of all, NACA 0012 airfoil with 160 coordinates points is used for the simulation, but the leading edge of that airfoil is not very smooth, which made it difficult to see the flow over the leading edge. Later the same airfoil is used but this time coordinates were increased to 400, which had a smooth leading edge, which is shown in the figures below.
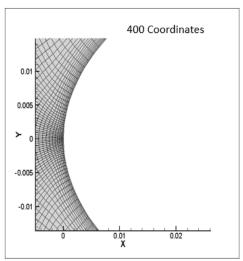

Fig. 4 Airfoil with 160 and 400 coordinates

V. PARAMETERIZATION AND OPTIMIZATION

Optimization of the airfoil is quite important and it can be achieved through a different approach. The part responsible for producing the lift for any type of aircraft or MAV is airfoils. Different airfoils have different features. Some airfoils create more lifts, some produce fewer drags, and some blend the two. Engineers also seek to create newly engineered airfoils that will have stronger aerodynamic properties than before.

The geometric form of the airfoil must be disrupted during the airfoil optimization process. There are several parameterization methods in use these days. Many approaches prove beneficial over others in terms of the convergence rate, the airfoil spectrum that could be described, etc. The parameterization method should minimize the number of parameters as possible, and it should be easy to generate and formulate [12]. In this paper Parsec method is used to optimize the airfoil with the help of Python code.

A. Parsec Parameterization Method

In engineering design optimization is a very extensive discipline these days. Practically everything that is being designed can be optimized in some way. With today's effectiveness, computers may often outperform engineers in optimizing complex designs subject to complex purposes. Hence, engineers are leaving hand-tuning in favor of automatic optimization.

While choosing the parameterization method, there are plenty of things that need to be considered. The flexibility of the parameterization method is a crucial aspect. While optimizing, it is necessary to use more variables as possible because fewer variables may not provide accurate results. As explained before, flexibility and robustness are two of the critical points for parameterization. On the goal of design activity, these decisions are strongly dependent [13].

PARSEC is known as one of the most simple and effective methods in the field of airfoil optimization. Fig. 5 demonstrates the eleven elementary parameters of the PARSEC method, which are the leading edge radius (r_{LE}), upper and lower crest location ($X_{UP}Z_{UP}$, X_{LO}, Z_{LO}) and curvature (Z_{xxUP}, Z_{xxLO}), trailing edge coordinate (Z_{TE}) and direction (α_{TE}), trailing edge wedge angle (β_{TE}) and thickness (∇z_{TE}). A linear combination of shape functions is used to present the airfoil shape in this method:

$$z = \sum_{n=1}^{6} a_{n,k} x_k^{\frac{n-1}{2}}$$

To define an airfoil shape using the Parsec method, all the eleven design parameters should be set properly. The coefficients a_n are determined from defined geometric parameters. The airfoil is generally divided into upper and lower surfaces, and the different factors are derived by using the information of the points on each surface. The subscript k changes from 1 to 2 to consider the length on the upper and lower surfaces, respectively. The positions and the maximum curvature of upper and lower surfaces can be monitored efficiently, which helps to reduce or delay the frequency of the shock wave, and that can be accomplished using the parameters mentioned earlier. Nonetheless, between the maximum thickness point and the trailing edge at the trailing edge of the airfoil, PARSEC fits a smooth curve, which successively deactivates the essential changes in the curvature near the trailing edge. Even though it has decent control over the crucial parameters on the top and bottom airfoil surfaces, PARSEC does not possess sufficient dominance in controlling the trailing edge shape where significant flow phenomena can happen [14].

In this paper, too, the PARSEC method was used to optimize the NACA 0012 airfoil through python code. The original NACA 0012 and optimized one as shown in Fig. 6.
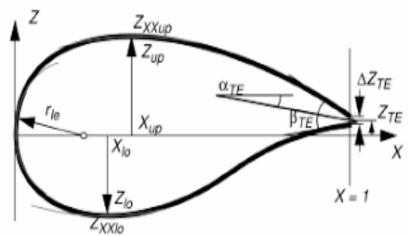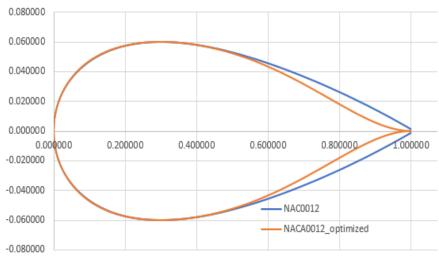

Fig. 5 Parsec method of parameterization

Fig. 6 Outlines for NACA 0012 and optimized NACA 0012

VI. NUMERICAL SIMULATION AND ANALYSIS

After generating the mesh, the airfoil simulation was completed, followed by the desired results. Xfoil calculations are taken as a reference value to compare with the results that are obtained from Fluent. Xfoil was then used to get different polar curves for NACA 0012 before comparing it to the results of Fluent.

A. Fluent CFD

The Unsteady Reynolds averaged Navier Stokes (URANS) method is used at 0.1s time step. The URANS methods used here provide greater flow field analysis in a considerably short time of a few hours on a typical desktop, and URANS simulations also help calculate the nonlinear dynamics of the entire flow field [15]. NACA 0012 airfoil with chord length 1m is simulated at low Reynolds number 200000 and Mach number 0.0086 to get aerodynamic characteristics at a different angle of attack. The turbulence model used for this simulation is the Spalart-Allmaras model under transient conditions. The Spalart–Allmaras model is a model that uses a one-equation to solve different problems. The SA model saves a considerable amount of computational effort compared to two-equation models like k-epsilon or k-ω while giving fairly good and more accurate results than the algebraic models. For the kinematic eddy turbulent viscosity, it solves a modeled transport equation [16]. The results obtained from Fluent for different AOA are compared with the reference values from XFOIL which is pretty close and satisfying as shown in the figures below.

Fig. 7 Lift coefficients and Drag coefficient of NACA 0012 in XFOIL and Fluent

NACA 0012 airfoil was later optimized using the Parsec method, as explained in chapter 4. Python code came in handy in optimizing the NACA 0012 airfoil. All the procedures that were applied to NACA 0012 airfoils were used for the optimized one too. As before, an O-grid structural mesh was created, and Xfoil values are taken as reference values. Similarly, 2D airfoil simulation is conducted in Fluent using URANS and Spalart Allmaras method; then the results are compared with the normal NACA 0012 and Xfoil, which are shown in the figures below.
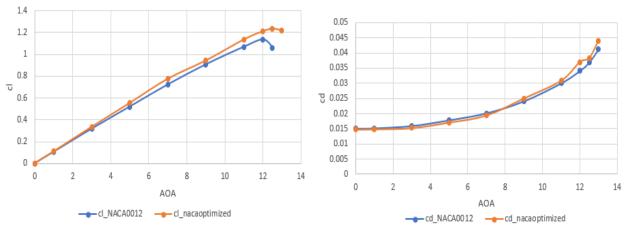
Fig. 8 Lift coefficient and Drag coefficient between NACA 0012 and Optimized NACA 0012 in Fluent
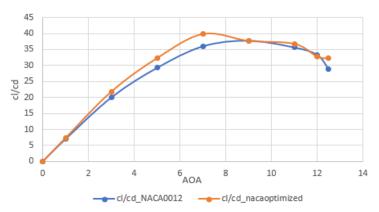

Fig. 9 Lift to Drag ratio between NACA 0012 and Optimized NACA 0012 in Fluent

The comparison between standard and optimized airfoil is made based on results obtained from CFD Fluent. Figure 8 and Figure 9 show the lift coefficient, drag coefficient, and lift-to-drag ratio for standard and optimized airfoil from Fluent, and the optimized airfoil has a better result than the standard one. So that we can say the optimization of the airfoil is successful.

The lift and drag coefficient graph for optimized airfoil is drawn below by comparing the results obtained from Xfoil and fluent. By looking at the chart, we can say that the results are pretty good.

Fig. 11 Comparison of Drag coefficients between Xfoil and Fluent for optimized airfoil

A pressure coefficient is a dimensionless number. In fluid dynamics, it describes the pressure relative to each point in the flow field. Each point in the flow field has its own pressure coefficient, which is denoted by Cp. The airfoil generates lift because of the pressure difference between the pressure(lower) and the suction(upper) surface. The pressure coefficient in the suction surface is negative, and the pressure surface is positive; that is why the airfoil's lift force is in the upward direction.

The graphs of pressure coefficient to the chord length of an airfoil NACA 0012 at a 7° angle of attack and 200000

Fig. 10 Comparison of lift coefficients between Xfoil and Fluent for optimized airfoil

Reynolds number for Xfoil and Fluent are shown below in Figure 12. Figure 13 is the same graph between NACA 0012 and optimized NACA 0012 at the same Reynolds number and angle of attack followed by Figure 14, which is the graph between pressure coefficient and chord length for optimized NACA 0012 in Xfoil and Fluent.
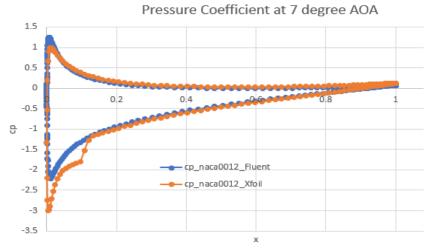

Fig. 12 Pressure coefficient comparison of NACA 0012 between Xfoil and Fluent

Fig. 13 Pressure coefficient comparison between NACA 0012 and Optimized NACA 0012

Fig. 14 Pressure coefficient comparison of optimized NACA 0012 between Xfoil and Fluent

From all the above pressure coefficient graphs, we can see that the graphs obtained from Xfoil have little flow separation, but the graphs obtained by the experiment from fluent seem smooth without any flow separation at 7° AOA.

31

B. Post-Processing

After getting results from CFD analysis, many flow-field variables can be used in post-processing for a better understanding of the flow over the airfoil or any other structure, such as vorticity magnitude, density, temperature, pressure, and pressure coefficient. The Q-criterion is one of the most widely used methods for vortex identification. In simple terms, the criterion identifies as vortices those regions where vorticity magnitude is larger than the strain-rate magnitude, or more precisely, where their difference is positive. Among the main advantages of the Q-criterion are its simplicity and straightforward application [17]. In this paper, NACA 0012 airfoil is used for simulation and optimization purposes. Different flow field variables are calculated for standard and optimized airfoils at 7° AOA and 200000 Reynolds numbers, which are shown below.

From the density distribution graph (Figure 15), we can see that it doesn't change relative to the chord length. Hence, the flow is incompressible.
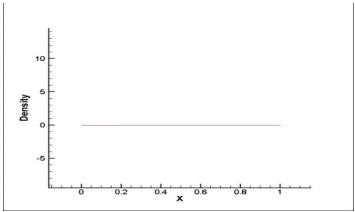

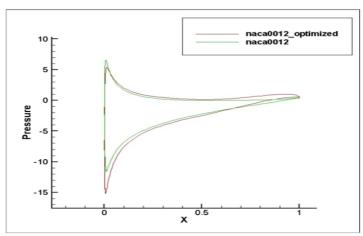Fig. 15 Density distribution for NACA 0012 and optimized airfoilat 7° AOA

Fig. 16 Pressure distribution for NACA 0012 and optimized airfoil at 7° AOA
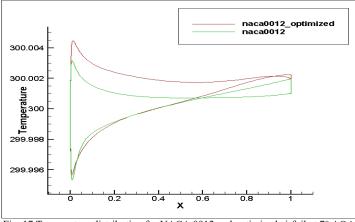

Fig. 17 Temperature distribution for NACA 0012 and optimized airfoil at 7° AOA

From this graph (Figure 16), we can conclude that the pressure distribution on the optimized airfoil is better than the NACA 0012. For the optimized airfoil, on the upper surface, the pressure distribution is more negative, and on the lower surface, it is more positive compared to NACA 0012. Since the pressure difference is more in an optimized airfoil, it can create more lift than that of NACA 0012.

If we observe the temperature distribution (Figure 17) over these two airfoils, there is not much of a difference. The reason behind this must be the viscous flow, because of which the friction force magnitude is not very big, resulting in a tiny temperature increment.

Fig. 18 Vortex generation by Q-criterion for NACA 0012 and optimized airfoil at 7° AOA

Looking at the Q-criterion of two different airfoils, we can easily conclude that the vortex generation at the trailing edge in NACA 0012 (left) is bigger than the optimized one. Hence,

the optimized airfoil has a reduction of drag compared to the original NACA 0102. Other variables showed better characteristics in an optimized airfoil as well.
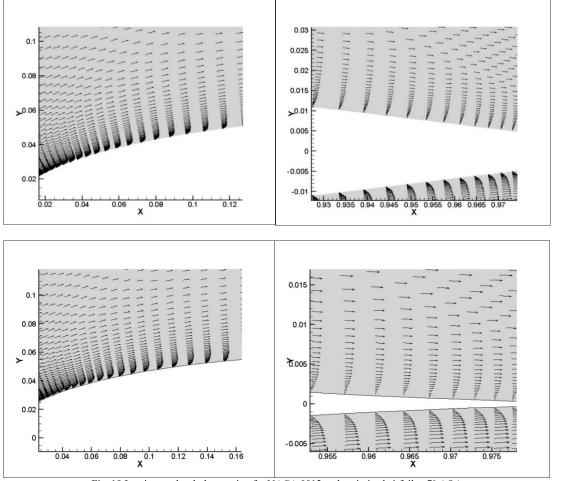

Fig. 19 Laminar and turbulent region for NACA 0012 and optimized airfoil at 7° AOA

As we can see in the pictures, both the airfoils flow tend to be laminar at the leading edge and turbulent at the trailing side. Since there is a very low adverse pressure gradient, the flow separation is not seen.
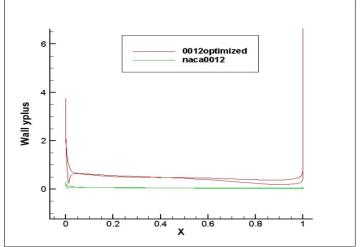

Fig. 20 Wall Y-plus values for NACA 0012 and NACA 0012 optimized at 7° AOA

For the optimized airfoil wall, yplus value is better than the NACA 0012. Yplus value for optimized airfoil is close to 1 or bigger than one, but for the standard airfoil, it is less than 1 or close to 1, which shows that the yplus value for optimized airfoil is better.

As we can see at 7° AOA, there is no reverse flow over the airfoil, but if you look at these two airfoils at 11° AOA, we can see the adverse pressure gradient and the flow separation. At 11° AOA, there is reverse flow, as we can see in the following pictures. At the trailing edge region, the flow separated and reattached.
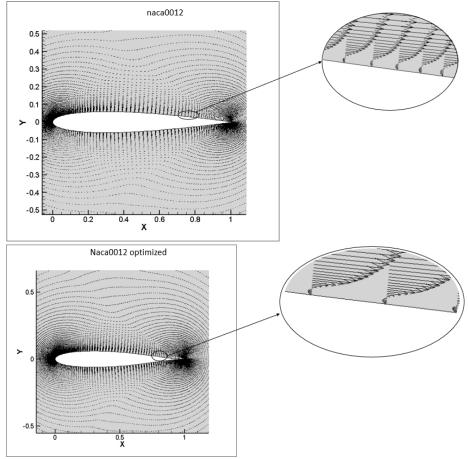

Fig. 21 Adverse Pressure Gradient effect for NACA 0012 and optimized airfoil at 11° AOA
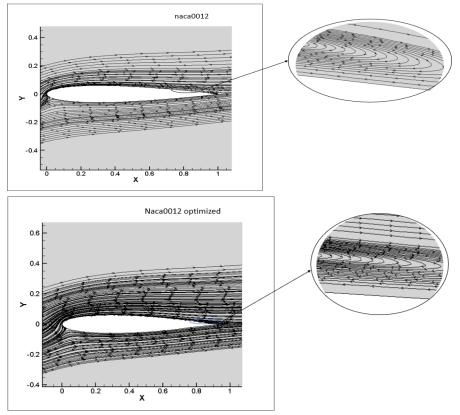
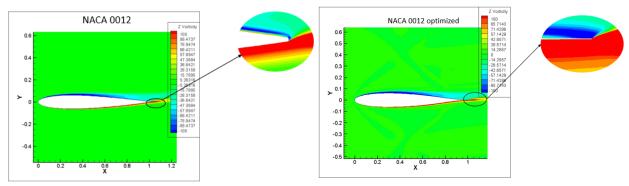Fig. 22 Reverse flow region for NACA 0012 and optimized airfoil at 11° AOA

Fig. 23 Z-vorticity for NACA 0012 and optimized airfoil at 11° AOA

Similarly, different variables at 11° and 20° AOA for NACA 0012 airfoil are compared to analyze its performance. At a higher angle of attack, we can see the separation of flow very clearly. Which are shown in the figures below.
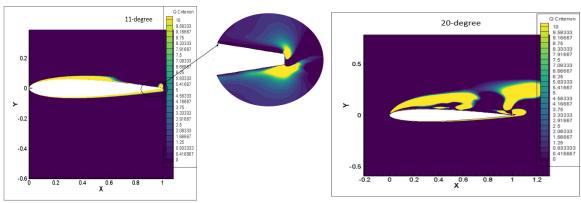

Fig. 24 Vortex generation by Q-criterion for NACA 0012 at 11° and 20° AOA

In these figures, we can see the vortex generation at 11° and 20° AOA. The magnitude of the vortex at 11° is very small compared to the 20°AOA. As AOA increases, the flow separation will happen very early, creating big vortices.
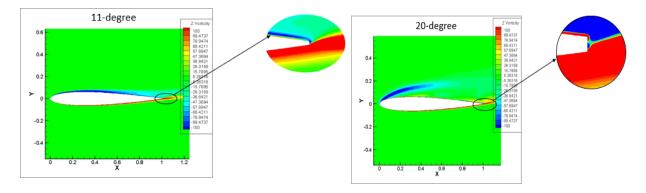

Fig. 25 Z vorticity magnitude for NACA 0012 at 11° and 20° AOA

Figure 25 is also associated with vortices. Here we can see the vortex magnitude in the Z direction. Different colors separate the different magnitudes and we can see that the vortex magnitude at 20° is larger compared to 11°.
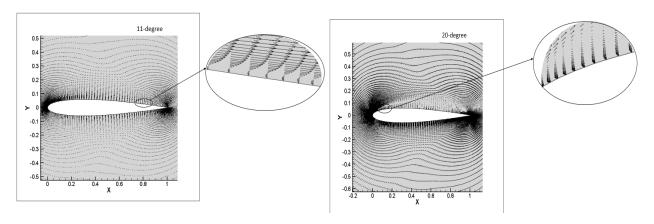

Fig. 26 Adverse Pressure Gradient for NACA 0012 at 11° and 20° AOA
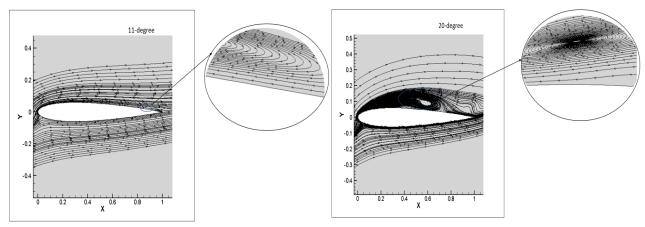

Fig. 27 Reverse flow (using Streamline) for NACA 0012 at 11° and 20° AOA

From figures 26 and 27, we can explain the difference between flow separation at 11° and 20° AOA, which is caused by an adverse pressure gradient. As we can see, at 11°, adverse pressure gradient is very small, which causes the flow separation at the trailing edge, and the separation is not so large. But, as AOA increases, the adverse pressure gradient will increase, and that causes the separation of flow at the leading edge, moreover, the flow separation is also very large compared to the moderate or lower angle of attack, which we can see in the figure at 20° AOA. At 20° reattachment will happen very late compared to 11°, which creates a big separation bubble.
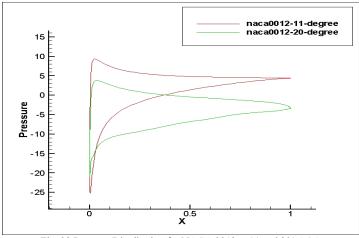
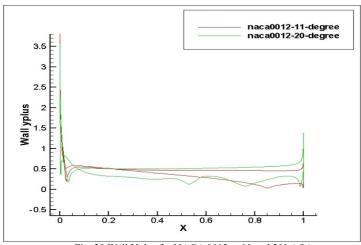Fig. 28 Pressure Distribution for NACA 0012 at 11 and 20° AOA

Fig. 29 Wall Yplus for NACA 0012 at 11 and 20° AOA

Figure 28 shows the pressure distribution at 11° and 20° AOA. We can see the separation bubble using streamlines, and we should be able to see this using a pressure graph too. But the separation cannot be seen in this graph, maybe because the mesh is not very dense on the leading and trailing edges. Similarly, from Figure 29, we can see that the airfoil at 20° AOA has a better wall yplus value than at 11° as it is closer to 1

VII. CONCLUSION

This work aimed to simulate a NACA 0012 airfoil at low Reynolds numbers for a different angle of attack before optimizing it to get better aerodynamic performances. Different aerodynamic characteristics for NACA 0012 airfoil are calculated using the CFD method in Ansys Fluent, which were later compared with the Xfoil results. These results are quite close, which shows that this simulation is successful. A similar process was followed for the optimized NACA 0012 airfoil. NACA 0012 airfoil was optimized using Python code by the Parsec method. For the optimized airfoil, the same aerodynamic characteristics were calculated and compared with the original airfoil, and the airfoil with improved aerodynamic properties was obtained. From the analysis, it was clear that the effect of an adverse pressure gradient was not seen at a lower angle of an attack like 7°. For moderate AOA like 11-degree, it has shown the effect of adverse pressure gradient with small reverse flow. As AOA increases, we can see the large reverse flow and flow separation, which were seen at 20° AOA. A NACA 0012 airfoil was simulated using the CFD method to analyze the different properties. Still, in the real world, other methods are implied to study those characteristics, such as Wind Tunnel testing. Overall, this paper was of success, as the results are quite satisfying.

REFERENCES

[1] W. J. Koning, E. A. Romander, and W. Johnson, "Low Reynolds number airfoil evaluation for the Mars helicopter rotor," in *Annual Forum and Technology Display*, No. ARC-E-DAA-TN53889, 2018.

[2] D. K. S. A. M. Sudipto, "Modeling aerodynamics for ultra-low Reynolds Number flight," in *21th Annual CFD Symposium*, Bangalore, India, August, 2019.

[3] T. I. Attari, "CFD analysis and validation for solution to micro air vehicle airframes," 2004.

[4] K. Shravan and N. Swaroop, "Numerical Investigation of an Airfoil at Low Reynolds Numbers for MAV Application," in *International Conference on Recent Advances in Design, Development and Operation of Micro Air Vehicles*, Hyderabad, India, November, 2014.

[5] L. W. Traub and C. J. J. O. A. Coffman, "Efficient low-Reynolds-number airfoils," Vol. 56, No. 5, pp. 1987-2003, 2019.

[6] I. A. A. S. V. R. Selwyn, "Design of Low Reynolds Number Airfoil for Micro Aerial Vehicle," in *IOP Conference Series: Materials Science and Engineering*, June 2018.

[7] S. Thabet, T. H. J. I. J. O. R. Thabit, and Engineering, "Computational fluid dynamics: science of the future," Vol. 5, No. 6, pp. 430-433, 2018.

[8] Y. D. A. J. R. R. . K. Raman, "A review on applications of computational fluid dynamics," *International Journal of LNCT,* Vol. No. 2, July, 2018.

[9] J. Anderson, in *Computational Fluid Dynamics-An Introduction Governing Equations of Fluid Dynamics*   3rd edition ed.: Springer, 2009, pp. 26-39.

[10] F. Aqilah, M. Islam, F. Juretic, J. Guerrero, D. Wood, and F. N. J. I. E. J. Ani, "Study of Mesh Quality Improvement for CFD Analysis of an Airfoil," Vol. 19, No. 2, pp. 203-212, 2018.

[11] J. F. G. Dias, Vicente, Akwa and Adriane Prisco Petry, "A Computational Study of the Grid Quality and Convergence in 2D Airfoils for Small Wind Turbine," in *15th Brazilian Congress of Thermal Sciences and Engineering*, Belém, Brazil, November, 2014.

[12] N. P. Salunke, R. Juned Ahamad and S. J. A. J. O. M. E. Channiwala, "Airfoil parameterization techniques: A review," Vol. 2, No. 4, pp. 99-102, 2014.

[13] W. Song and A. Keane, "A study of shape parameterisation methods for airfoil optimisation," in *10th AIAA/ISSMO multidisciplinary analysis and optimization conference*, pp. 4482, 2004.

[14] A. Shahrokhi, A. J. A. s. Jahangirian, and technology, "Airfoil shape parameterization for optimum Navier–Stokes design with genetic algorithm," Vol. 11, No. 6, pp. 443-450, 2007.

[15] M. W. Lohry and L. J. A. J. Martinelli, "Unsteady Reynolds-averaged Navier–Stokes simulation of crossflow rotors, scaling, and blockage effects," Vol. 54, No. 12, pp. 3828-3839, 2016.

[16] P. V. Raje, "Spalart-Allmaras Turbulence Model For Compressible flows," Indian Institute of Technology, Bombay, India, May, 2015.

[17] V. Kolář and J. J. I. J. O. A. E. Šístek, "Vortex and the balance between vorticity and strain rate," 2019.